Construction of prognostic model and tumor microenvironment landscape based on cuproptosis-related subtypes in melanoma

Authors

Zishen Xia, Nan Gao, Jianwen Wang, Lizhao Yan, Cong Ma, Kangwei Wang, Yuxiong Weng

Correspondence

yxweng1218@163.com (Y. Weng)

Graphical Abstract

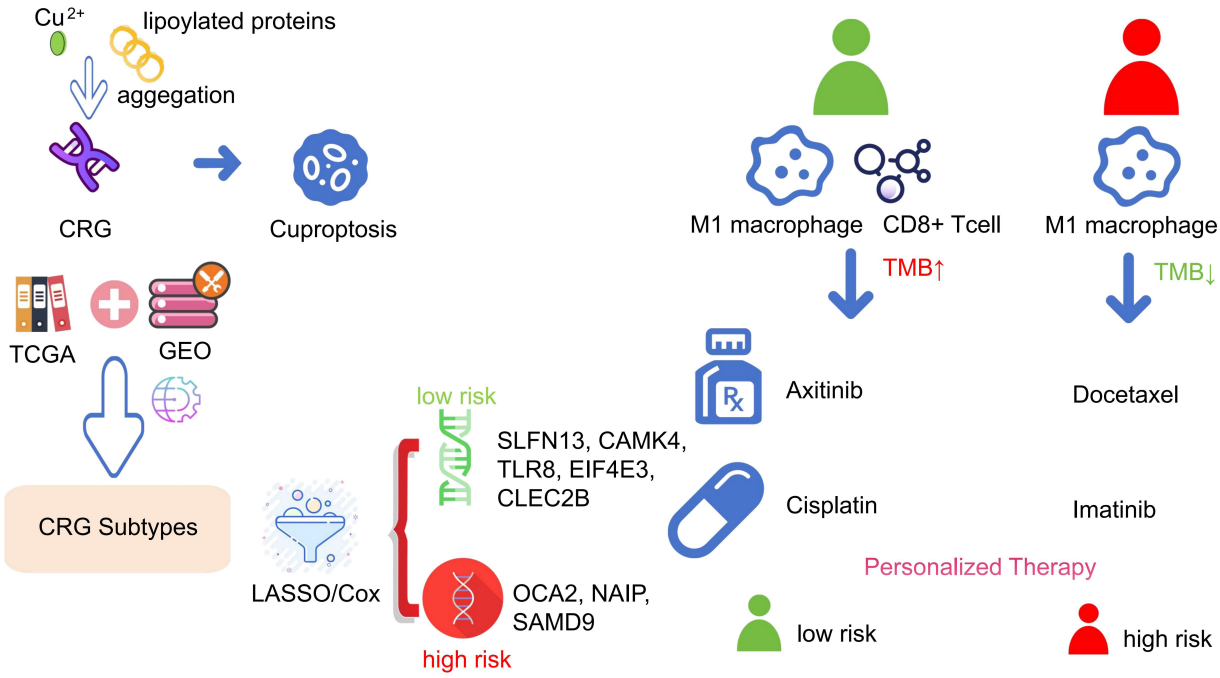

https://doi.org/10.71321/vxy0xd87

Research Article Life Conflux

Construction of prognostic model and tumor microenvironment landscape based on cuproptosis-related subtypes in melanoma

Zishen Xia[1†], Nan Gao[1†], Jianwen Wang[1†], Lizhao Yan[1], Cong Ma[1], Kangwei Wang[1], Yuxiong Weng[1*]

Received: 2025-04-22 | Accepted: 2025-08-30 | Published online: 2025-10-13

Abstract

Background: Melanoma, known for its aggressive nature and poor prognosis, may be impacted by cuproptosis, a recently discovered form of programmed cell death. Despite its unclear mechanisms, preliminary studies suggested a link between cuproptosis and cancer progression and metastasis. We aimed to investigate the association between cuproptosis-related genes (CRGs) and melanoma to enhance prognostic and therapeutic strategies.

Method: In this study, we downloaded transcriptome RNA-seqs and clinical information of all melanoma patients from The Cancer Genome Atlas (TCGA) database, selected a dataset from Gene Expression Omnibus (GEO) databases, and merged the two datasets. After univariate regression analysis, all the samples were categorized into three groups based on expression levels of CRGs. Differential expression analysis was carried out for three CRG clusters to obtain the significant differentially expressed genes (DEGs). After univariate Cox regression analysis, multivariate Cox regression analysis and the least absolute shrinkage and selection operator (LASSO) algorithm were performed on DEGs, the prognosis related genes were screened to establish a prognosis prediction model. The model's accuracy was validated through Kaplan-Meier analysis, receiver operating characteristic (ROC) curve, nomogram, and independent prognostic analysis. Additionally, we compared the immune scores of the tumor microenvironment, tumor mutation burden, tumor immune dysfunction and exclusion, and drug sensitivity between high-risk and low-risk groups.

Results: Through algorithm analysis, eight genes significantly related to prognosis were identified, among which SLFN13, CAMK4, TLR8, EIF4E3, and CLEC2B were low-risk genes, OCA2, NAIP, and SAMD9 were high-risk genes. Using these genes, we established a prognostic model that effectively distinguishes between different survival outcomes, with the low-risk group showing a markedly higher long-term survival rate.

Conclusion: In conclusion, based on the research of cuproptosis subtypes, we identify the DEG with predictive potential and establish a prognosis prediction model. This study may provide a reference for the prognosis and clinical treatment of melanoma patients from the perspective of cuproptosis.

Keywords: melanoma; cuproptosis; tumor microenvironment; differentially expressed genes; risk score; bioinformatics analysis.

Introduction

Melanoma, a malignant tumor that originates from melanocytes, typically manifests in the skin [1,2]. The development of melanoma is influenced by both environmental and genetic factors [3]. Often resembling melanocytic nevi, its early symptoms can be subtle, complicating early detection and diagnosis [4]. By the time symptoms appear, melanoma frequently advances to a late stage characterized by rapid progression, widespread metastasis, and poor prognosis [5, 6].

The primary treatment for metastatic melanoma has long been surgical resection combined with chemotherapy [7]. For decades, immunotherapy and targeted drugs, such as PD1 – PDL1 inhibitors, small molecule BRAF and MEK inhibitors, cytotoxic T lymphocyte antigen 4 (CTLA4) inhibitors, and the combination of multiple drugs have been explored to revolutionize the treatment of malignant melanoma [8, 9]. However, not all melanoma patients respond effectively [10], and resistance to these therapies is emerging [11]. This underscores the critical need for new biomarkers that can predict prognosis and effective therapeutic targets.

Copper, an essential trace element, plays a pivotal role in various cellular functions due to its inherent redox properties [12], serving as a cofactor for enzymes involved in mitochondrial respiration, antioxidant defense, and the biosynthesis of hormones, neurotransmitters, and pigments [13]. Recent studies have highlighted that disruptions in copper homeostasis can lead to cytotoxic effects [14-16]. Tsvetkov et al. showed a unique cell programmed death mode caused by excessive copper accumulation called cuproptosis [17]. This process involves the binding of excess copper to lipoylated proteins

1 Department of Hand Surgery, Union Hospital, Tongji Medical College, Huazhong University of Science and Technology, Wuhan, China

† These authors contributed equally to this work.

* Corresponding Author.

in the tricarboxylic acid (TCA) cycle, triggering protein aggregation, loss of Fe-S cluster proteins, and resultant proteotoxic stress. Interestingly, previous studies have shown that cancer cells exhibit higher copper levels than normal tissues, suggesting that they exploit copper for energy needs while avoiding cuproptosis [13, 18, 19]. This seems to offer a potential therapeutic avenue targeting copper metabolism in cancer cells.

In this study, we aimed to define the role of cuproptosis in melanoma by analyzing cuproptosis-related gene (CRG) expression in patient samples. We categorized melanoma patients based on CRG expression profiles into distinct subtypes, assessed their immune characteristics, and developed a new prognostic model using differentially expressed genes (DEGs) linked to these CRG clusters. This approach may provide valuable insights for enhancing melanoma diagnosis and treatment strategies.

Materials and Methods

Data Collection and Preparation

Transcriptomic RNA-seq and clinical data were acquired from The Cancer Genome Atlas (TCGA) database and the GSE65904 dataset from Gene Expression Omnibus (GEO). After screening, samples lacking complete survival information or from normal tissues were excluded. The remaining transcriptomic and clinical data were merged from both sources. Additionally, somatic mutation and copy number variation (CNV) were downloaded from GDC and UCSC Xena, respectively. We utilized 18 CRGs (NFE2L2, NLRP3, ATP7B, ATP7A, SLC31A1, FDX1, LIAS, LIPT1, DLD, DLAT, PDHA1, PDHB, MTF1, GLS, CDKN2A, DBT, GCSH, DLST) identified from previous studies [13, 17, 18, 20, 21].

CNV analysis and prognosis analysis of CRGs

CNV of CRGs was extracted from the CNV file downloaded from TCGA. We analyzed the difference and used the R package "RCircos" (version 1.2.2) for visualization. To validate the prognostic value of CRGs, survival analysis and univariate Cox regression analysis were conducted on the merged data using the R package "limma" (version 3.64.3) and "survival" (version 3.8.3). According to the relationship between high and low gene expression and survival information, CRGs were divided into "Favorable factors" and "Risk factors".

Consensus clustering analysis with CRGs

R package "ConsensusClusterPlus" (version 1.58.0) was run to cluster the expression differences of these 18 CRGs in the merged sample dataset. The samples were divided into different clusters based on the result of cuproptosis clustering. Kaplan-Meier analysis was conducted to compare survival probability differences among different CRG clusters. In addition, the principal component analysis (PCA) diagram showed the geometric distance between subclusters. The heatmap showed the difference of CRGs expression. Gene set variation analysis (GSVA) was conducted to present the differences in immune pathway enrichment between the three clusters. Single sample gene-set enrichment analysis (ssGSEA) algorithm was performed to compare the immune cell infiltration of different CRG clusters, and we visualized the results with R package "ggpubr" (version 0.6.1).

Identification of CRG clusters related DEGs and function enrichment analysis

Differential expression analysis was carried out for three CRG clusters to obtain the DEGs. The intersection of DEGs across the three clusters was further analyzed. GO and KEGG function enrichment analyses were conducted for these DEGs.

Obtaining DEG clusters

We performed univariate Cox regression analysis on the DEGs to get the significant DEGs and conducted the consensus unsupervised clustering analysis for these DEGs. The merged sample data was divided into different DEG clusters. Kaplan-Meier (K-M) survival analysis was performed to show the survival differences among DEG clusters. The heat map was drawn to describe the differential expression of DEG clusters, and the boxplot described the differential expression of CRGs among DEG clusters.

Prognostic Model Construction and Validation

Prognostic genes were determined using multivariate Cox regression, and LASSO algorithm. To prevent overfitting, the optimal penalty coefficient was obtained through cross validation of 1000 iterations. The prognostic CRG clusters related DEGs optimal group was determined, and a prognostic risk model was established using multivariate Cox regression from DEG signature, with patients' risk scores calculated as follows: Risk score = $\sum_{i=1}^{n}$ exp (Xi) * coef (Xi), "exp" means gene's expression, "coef" means corresponding coefficient. The patients were randomly divided into training and test sets (1:1 ratio), and the training set, the test set, and all patients were further divided into high-risk and low-risk groups based on median risk scores, respectively. Kaplan-Meier analysis was carried out by "survival" R package to compare the long-term survival probability between the training set, test set, low-risk group, and all patients. In addition, based on the "survival" (version 3.8.3), "survminer" (version 0.4.2), "timeROC" (version 0.4) R package, we created the receiver operating characteristic (ROC) curves of 1-, 3-, and 5- years and calculated the area under the curve (AUC) to compare the testing effectiveness.

Establishment of Predictive Nomogram

We combined various key clinical factors with risk scores and used the "rms", "regplot" R package to construct 1-year, 3-year, and 5-year nomographs to predict the long-term survival rate of melanoma patients. And to verify the reliability of the model, we drew a calibration curve according to the Hosmer – Lemeshow test. The independence of the prognostic model from clinical factors such as sex, age, and pathological stage was confirmed through univariate regression and multivariate regression analysis.

Analysis of immune microenvironment (TME), tumor mutation burden (TMB), and tumor immune dysfunction and exclusion (TIDE)

The CIBERSORT method was used to analyze the difference in immune infiltration of total melanoma samples. We used the R package "ESTIMATE" to evaluate immune scores, stromal scores, and estimate scores of TME. This algorithm can use gene expression characteristics to estimate the level of stromal cells and immune cells in malignant tumor tissues. We also run the "maftools" R package (version 2.24.0) to analyze

the TMB and compare the gene mutation differences between high-risk group and low-risk group. And TIDE was downloaded from TIDE website (http://tide.dfci.harvard.edu) to predict patients' response to immunotherapy [22, 23].

Drug sensitivity analysis

According to the Genomics of Drug Sensitivity in Cancer (GDSC, https://www.cancerrxgene.org/) database, the "pRRophetic" package (version 0.5) in R was applied to compare the difference between high-risk groups and low-risk groups in sensitivity to chemotherapy drugs.

Statistical analysis

All statistical analyses in this study were performed using R software (version 3.6.1) and PERL. A p-value of less than 0.05 (two-sided) was considered to indicate statistically significant differences. Univariate Cox regression analysis was utilized to identify DEGs with prognostic value. We constructed the prognostic prediction model using the LASSO regression algorithm, univariate Cox regression analysis, and multivariate Cox regression analysis.

Result

CNV and prognosis value of CRGs

Analysis of the CNV in 18 CRGs highlighted significant reductions in CDKN2A, DLAT, GCSH, FDX1, and DBT, with increases observed in NLRP3. These variations suggested distinct patterns of transcription and expression of CRGs in tumor samples (Figure 1A), potentially reflecting their involvement in tumor development, progression, or other molecular mechanisms. Chromosomal locations of CRGs, with increases marked in red and decreases in blue, are displayed in Figure1B. To further assess the prognostic significance of these CRGs, we integrated transcriptome RNA sequencing data with clinical information from the TCGA and GEO databases and conducted Kaplan-Meier survival analysis. The analysis revealed

Figure 1. Genomic variation of CRG. (**A**) The change of CNV frequency of CRGs. (**B**) CRG position of CNV on the chromosome. (**C**) The interaction between CRGs in melanoma, where the width of the line represents the strength of the correlation between CRGs.

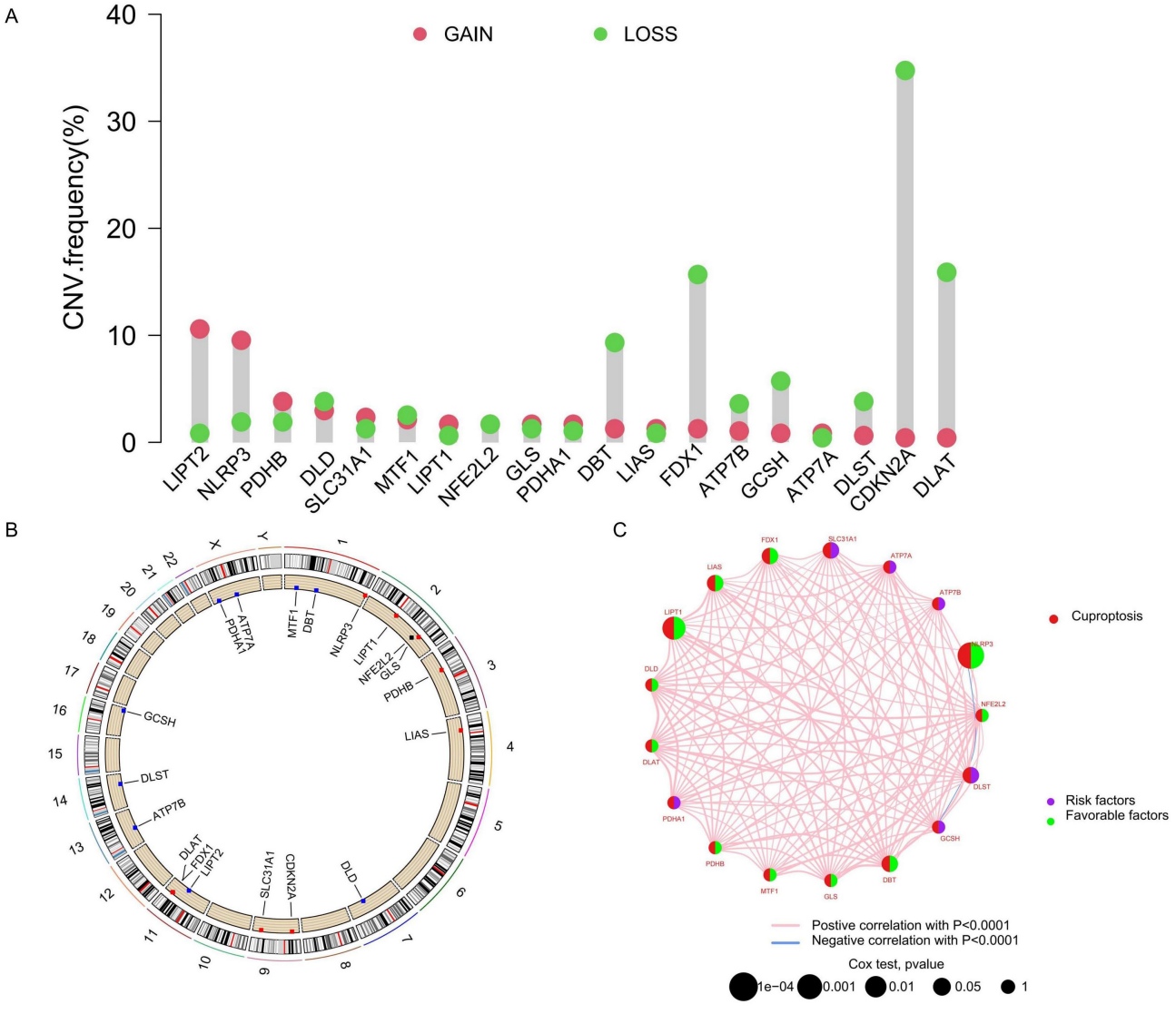

significant differences in overall survival between high and low expression groups for 15 CRGs, including ATP7A, ATP7B, CDKN2A, DBT, DLD, DLST, FDX1, GCSH, LIAS, LIPT1, MTF1, NFE2L2, NLRP3, PDHA1, and SLC31A1 (see Supplementary Figure S1A-O online). Based on the survival curves from this analysis, we categorized the CRGs into "Risk factors" and "Favorable factors," which are illustrated in a network diagram (Figure 1C).

Consensus clustering analysis with CRGs

To clearly delineate the characteristic distribution of CRGs across varying expression levels in all samples, we performed consensus clustering analysis on the transcriptome data, simulating group numbers from k=2 to k=9. The classification was most distinct at k=3, effectively reflecting the differences in expression and potential biological diversity among the samples. Consequently, we divided the samples into three CRG clusters: A (n=276), B (n=280), and C (n=126), based on their expression characteristics related to risk and Favorable factors (Figure 2A). PCA results revealed significant differences in gene expression profiles among the three CRG clusters (Figure 2B), suggesting that different clusters may represent distinct biological states. The heat map showed the differential expression of CRG among the three clusters and different clinical features (Figure 2C). Further, K-M survival analysis of the three CRG clusters indicated significant differences in survival outcomes, with CRG cluster A exhibiting a notably higher long-term survival probability than clusters B and C (Figure 2D). In addition, GSVA results highlighted the top 20 most significant pathways differing among clusters A, B, and C (see Supplementary Figure S2A-C online). Analysis of immune cell proportions in the three clusters was conducted using ssGSEA (Figure 2E). The results demonstrated varying types of immune cell infiltration across the melanoma samples, identifying potential therapeutic targets within these immunological variations

Identification of CRG clusters related DEGs and immune function enrichment analysis

Differential expression analysis across the three CRG clusters identified intersecting DEGs, presented in a Venn diagram (Figure 3A). Subsequent immune function enrichment analyses using GO and KEGG were conducted on these intersecting DEGs. The GO analysis identified significant enrichment in Molecular Function (MF) and Biological Process (BP) categories (Figure 3B, Supplementary Figure S3A). KEGG enrichment analysis further demonstrated significant differences in the expression of DEGs within cytokine-cytokine receptor interaction, Toll-like receptor signaling pathway, and PI3K-Akt signaling pathway, etc (Figure 3C, Supplementary Figure S3B). These findings highlight the significant impact of DEGs associated with CRG clusters on immune regulation within melanoma.

Obtaining DEGs clusters

Significant DEGs were obtained through univariate Cox regression analysis. Based on the expression differences, we conducted a grouping simulation, finding that categorizing the samples into two clusters (A and B) provided the most distinct grouping performance (Figure 4A). Subsequently, K-M survival analysis revealed that the long-term survival probability of

Figure 2. Identification and analysis of the CRG clusters. (**A**) Unsupervised consensus clustering identified three molecular subtypes of cuproptosis. (**B**) The PCA results show the distribution of the three CRG clusters. (**C**) It shows the differential expression of CRG among the three CRG clusters and different clinical features. (**D**) The K-M survival analysis of the 3 CRG clusters. (**E**) The immune infiltration difference of TME in the three clusters.

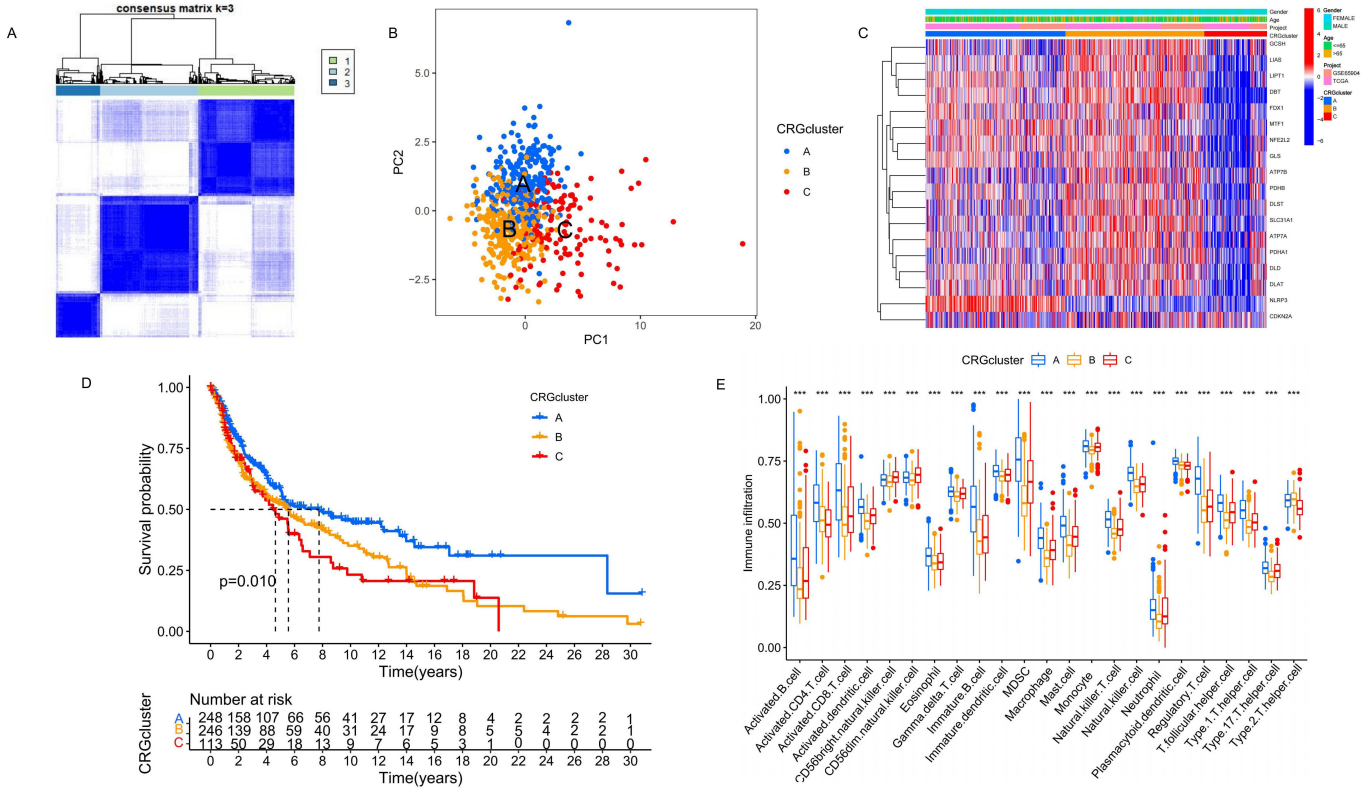

samples in cluster A was significantly higher than in cluster B (Figure 4B). Additionally, we combined the characteristic of CRG clusters and population drew a heatmap of gene expression differences (Figure 4C). The differences in CRG expression between the two DEG clusters were further detailed in a boxplot (Figure 4D), where risk factors such as ATP7B, DLST, GCSH, and PDHA1 showed notably higher expression in cluster B. These findings highlight the potential of these DEGs in predicting prognosis in melanoma patients, and also suggested the possible role of CRGs in melanoma progression.

Construction of prognostic model

The LASSO algorithm analysis and multivariate Cox regression analysis were applied to 293 DEGs intersecting across three CRG clusters, as shown in Figure 5A and 5B. After 1,000 iterations, this analysis identified a prognostic model composed of eight genes—SLFN13, CAMK4, TLR8, EIF4E3, CLEC2B, OCA2, NAIP, and SAMD9—which exhibited substantial prognostic relevance. The risk score for this model was calculated as follows: Risk score = exp (TLR8) × (-0.266) + exp (SAMD9) × 0.252 + exp (NAIP) × 0.465 + exp (EIF4E3) × (-0.152) + exp (CLEC2B) × (-0.271) + exp (SLFN13) × (-0.121) + exp (CAMK4) × (-0.103) + exp (OCA2) × 0.091. Using this signature, we calculated risk scores for all samples, classifying them into high and low-risk groups based on the median score. A Sankey diagram (Figure 5C) illustrated the relationships between CRG clusters, DEG clusters, risk groups, and survival outcomes, highlighting the efficacy of CRG and DEG classifications in predicting melanoma patient risk and survival. The boxplot showed the risk score variations in CRG clusters (Figure 5D) and DEG clusters (Figure 5E), revealing that groups with higher long-term survival probabilities, specifically CRG Cluster A and DEG Cluster A, had lower risk scores. Additionally, boxplots comparing high and low-risk groups (Figure 5F) showed significant differences in the expression of CRGs, where risk factors such as SLC31A1, ATP7A, ATP7B, DLST, GCSH, and PDHA1 are significantly elevated in the high-risk group. These findings underscore the reliability of our prognostic model.

Verification of the Prognostic Model

A total of 607 melanoma patients were randomly divided into a test set (303 samples) and a training set (304 samples), nearly a 1:1 ratio, to assess the effectiveness of the risk prediction model. K-M survival analysis was conducted on all samples, training set and test set categorized by high and low-risk groups, consistently showed that the long-term survival probability of the low-risk group was significantly higher than that of the high-risk group (Figure 6A-C). This finding confirmed that the risk prediction model effectively differentiates patients with varying prognostic levels. Expression differences of prognostic signature genes between the high-risk and low-risk groups were visualized using heatmaps across all samples, training, and test sets (Figure 6D-F). Scatter plots depicting the survival time against increasing risk scores indicated that higher scores were associated with a significant increase in mortality and a notable decrease in survival time (Figure 6G-L). To evaluate the sensitivity and specificity of the prognostic model, we drew the ROC curve, the AUC of 1-, 3- and 5-year were 0.680, 0.758, and 0.785 in training set, and the minimum AUC of all the samples and test set was 0.647 (Figure 6M-O). These results emphasize the model's strong predictive capability for long-term prognosis, even at the lowest AUC value.

Figure 3. GO and KEGG analysis of the CRG clusters related DEGs. (**A**) Intersection DEGs of three CRG clusters. (**B-C**) Visualization of GO and KEGG analysis results.

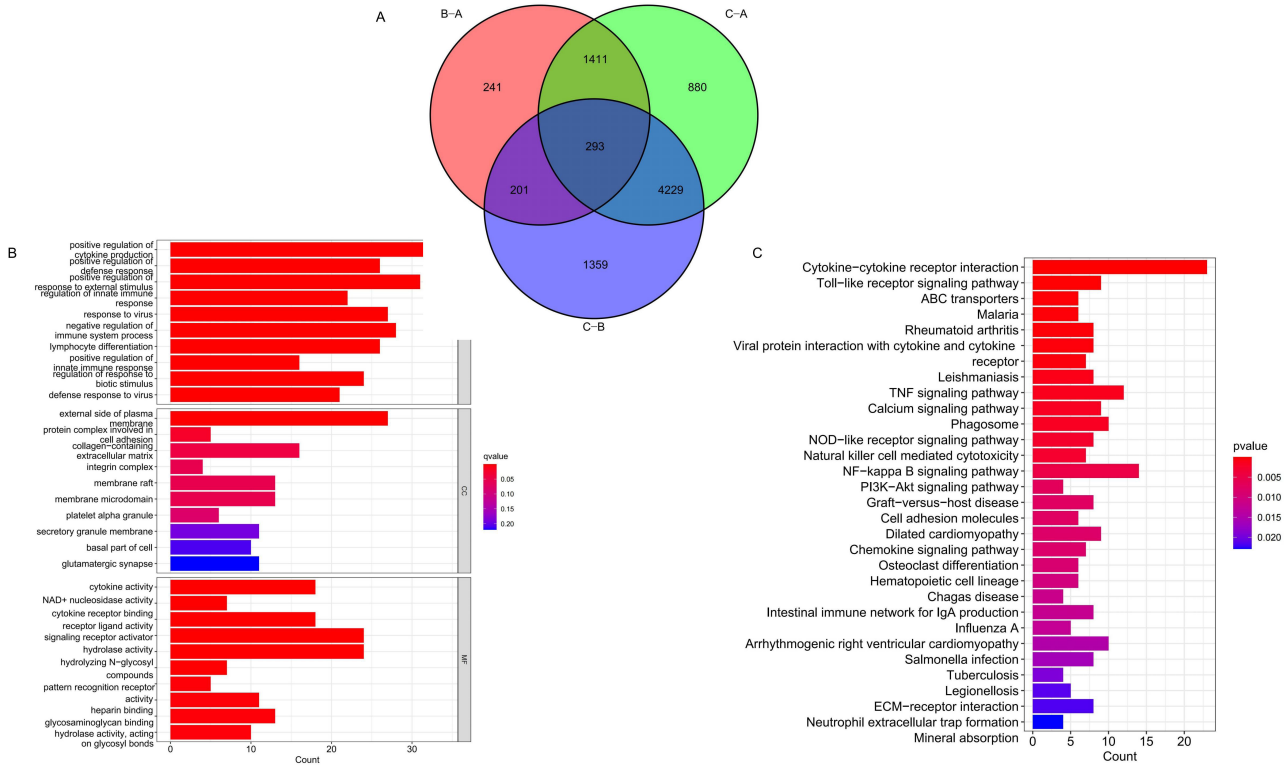

Further verification of the model's reliability as an independent predictor was conducted using univariate and multivariate Cox regression analyses. The hazard ratio (HR) values of risk score showed that it could be regarded as an independent prognostic indicator alongside clinical characteristics (Figure 7A-B). To enhance clinical applicability, a nomogram integrating clinicopathological features and risk scores was developed to quantitatively predict 1-year, 3-year, and 5-year survival probabilities for melanoma patients (Figure 7C). As shown in Figure 7C, if the total risk score of a patient is 258 points, then in the prediction of this model, the survival probability of this patient in the next 1 year, 3 years and 5 years is 90.5%, 46.8% and 28.3% respectively. The accuracy of the nomogram was affirmed by calibration curves, which showed high consistency between actual observations and predictions (Figure 7D). These findings suggest that the constructed risk prediction model not only effectively forecasts the survival prognosis of melanoma patients but also holds substantial potential for clinical application due to its high predictive accuracy and consistency.

Analysis of immune microenvironment, TMB and TIDE

To understand the relationship between prognostic genes, risk scores, and immune cell infiltration, we utilized the CIBERSORT algorithm (Figure 8A). The analysis revealed that higher risk scores were negatively correlated with the infiltration of M1 macrophages, plasma cells, activated CD4 memory T cells, and CD8 T cells, but positively correlated with M0 macrophages. This suggests that a higher risk score reflects a more immunosuppressive TME. Further evaluation of immune, stromal, and estimate scores within the TME showed significantly higher scores in the low-risk group compared to the high-risk group (Figure 8B). This indicated a more robust immune presence in the low-risk group, underscoring the importance of the TME in patient prognosis.

Immune checkpoint blockade (ICB) therapy has shown substantial clinical benefits in treating melanoma; however, its effectiveness varies, and some patients experience considerable side effects [24]. Recent studies have identified TMB as a valuable predictor of tumor immune response, potentially indicating the efficacy of ICB therapy [22, 25, 26]. Quantitative TMB analysis revealed that the high-risk group had a higher concentration of mutations across more genes than the low-risk group, which may correspond to a higher TMB (Figure 8C-D). K-M analysis further demonstrated that patients with high TMB had better survival probabilities than those with low TMB. Moreover, integrating risk model predictions, we found that the

Figure 4. Identification and analysis of the DEG clusters. (**A**) Unsupervised consensus clustering identified two DEG clusters. (**B**) The K-M survival analysis of the DEG clusters. (**C**) The clinical characteristics and cuproptosis subtypes differences between the two DEG subtypes. (**D**) The differences in CRG expression between the two DEG clusters.

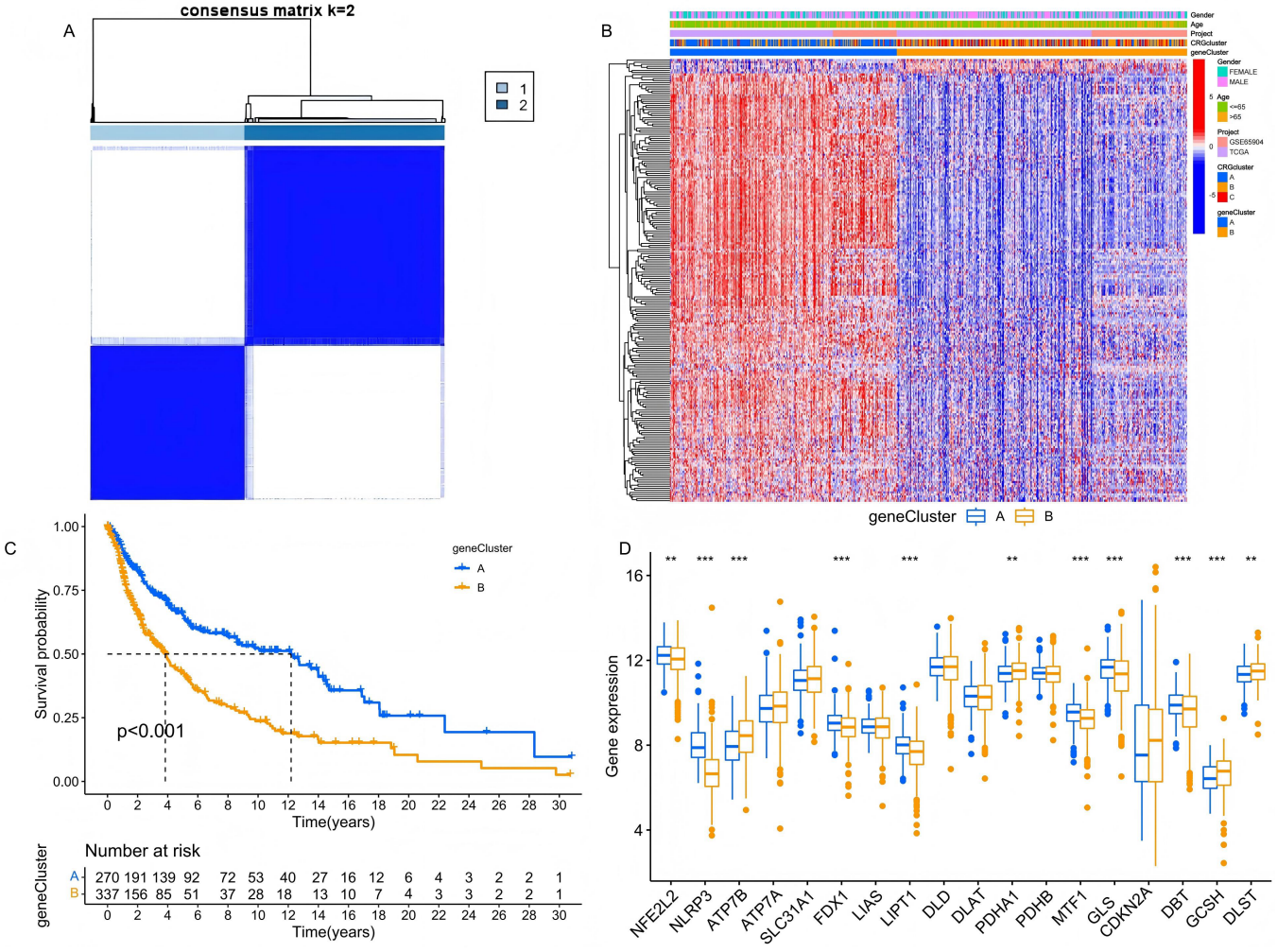

highest long-term survival probability was observed in patients with high TMB and low-risk scores, whereas the lowest was in those with low TMB and high-risk scores (Figure 8E-F).
Additionally, we obtained immunotherapy scores for patient samples from the TIDE website and conducted a matching analysis with our prognostic model, calculating TIDE scores for the two groups. The results showed significant differences in TIDE scores, with higher scores observed in the low-risk group compared to the high-risk group (Figure 8G). When combined with the TMB analysis, these results suggested that patients in the high-risk group may have a more active response to immunotherapy.

Drug sensitivity analysis

To enhance the clinical utility of our prognostic model and improve treatment efficacy, we compared the drug sensitivity between the high-risk and low-risk groups to identify potential drugs for more effective immune or targeted therapies. The analysis of half-maximal inhibitory concentration (IC50) for various drugs revealed significant differences between the two groups. The low-risk group demonstrated greater sensitivity to several immunotherapeutic and targeted drugs, including Axitinib, Cisplatin, Gemcitabine, Methotrexate, Nilotinib, Rapamycin, Sunitinib, and Temsirolimus (Figure 9A-H). Conversely, the high-risk group exhibited higher sensitivity to drugs such as Docetaxel, Elesclomol, Imatinib, and Thapsigargin (Figure 9I-L). These findings provided valuable insights into tailoring treatment strategies based on the risk profile, potentially leading to more effective therapeutic interventions for patients.

Discussion

Melanoma, the most prevalent and deadly form of skin cancer, often goes undetected in its early stages due to non-obvious symptoms, leading to diagnoses at more advanced stages with metastatic lesions and consequently poor prognoses [27, 28]. While the development and application of immunotherapy and targeted therapies, such as BRAF inhibitors, BRAF/MEK combination targeted therapy, and PD-1/PD-L1/CTLA-4 blockers, have significantly improved outcomes for many patients, resistance to these therapies frequently develops through mutations that promote irreversible drug resistance [10, 29, 30].
The progression of tumor cells is primarily driven by accumulations of gene mutations, which lead to uncontrolled cell proliferation [31]. A critical aspect of many cancers, including melanoma, is the activation of the MAPK pathway, which stimulates growth-promoting genes, leading to anchoring loss and inhibition of intercellular contact, resulting in uncontrolled cell proliferation and transformation [1, 32].Normally, cells can initiate various regulated cell death (RCD) mechanisms to maintain cellular homeostasis, including necroptosis, pyroptosis, ferroptosis, autophagic cell death, programmed cell death and apoptosis [33]. In addition, a novel form of cell death termed cuproptosis, characterized by copper-induced cell death, has been identified [17]. The research showed that excessive cop-

Figure 5. Construction of the prognostic model. (**A-B**) LASSO regression analysis screened prognostic signatures from the DEGs to build the model. (**C**) The relationship among CRG clusters, DEG clusters, risk groups and survival status. (**D**) Distribution of risk scores across the three CRG clusters. (**E**) Distribution of risk scores across the two DEG clusters. (**F**) Comparison of CRG expression between the high-risk group and low-risk group.

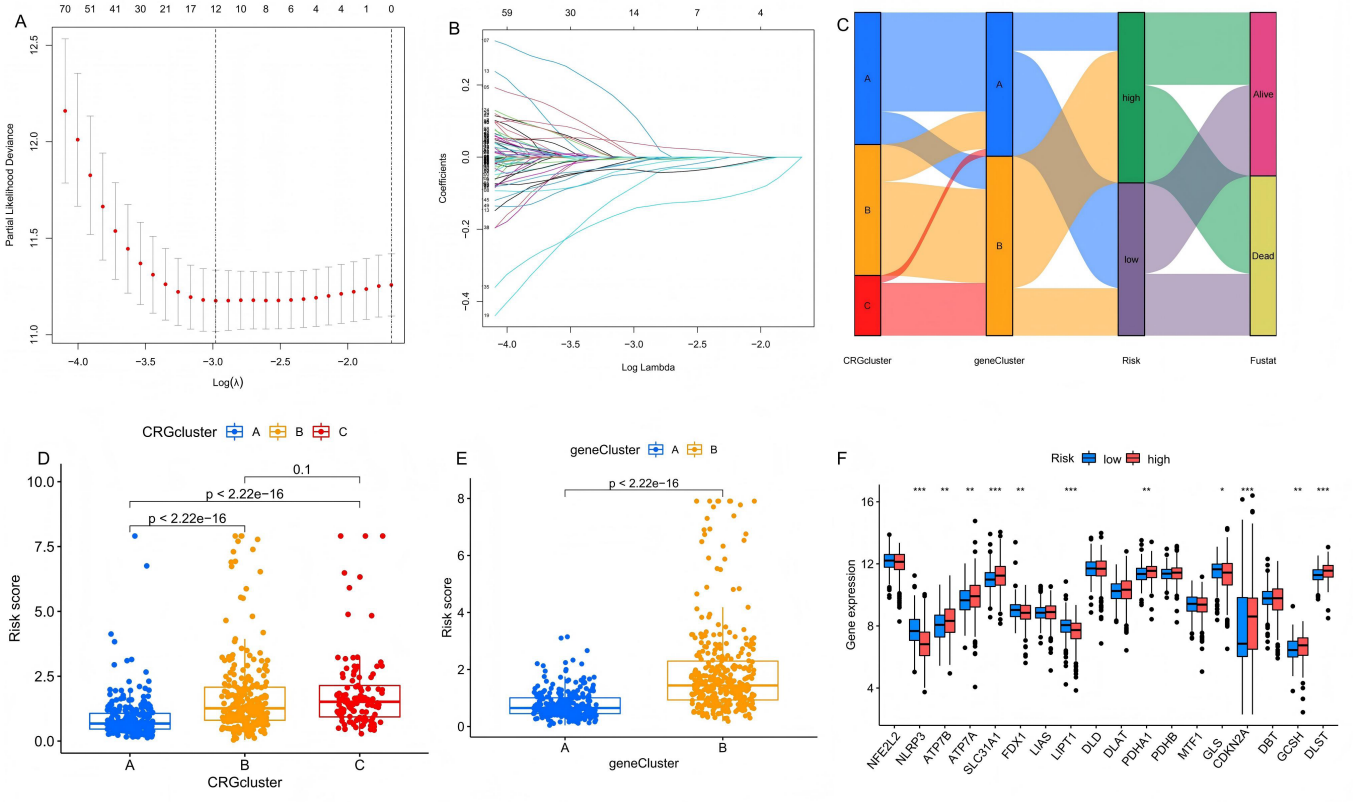

per accumulates in cells and directly combines with the lipoylated components of the TCA, leading to the aggregation of lipoylated proteins and the loss of Fe-S cluster proteins, which in turn leads to protein toxicity stress and eventually leads to cell death. And they proved that FDX1 (a cuproptosis related gene) was involved in regulating the lipoylation of proteins. In addition, the analysis of cancer dependency graph showed that the expression of FDX1 was positively correlated with the level of lipoic acid in tumor tissue, and the deletion of FDX1 could inhibit the lipoylation of dihydrolipoamide S-acetyltransferase (DLAT) (an enzyme in TCA). This showed that the new field of cuproptosis may provide a new perspective to develop therapeutic targets for cancer treatment.

In this study, we categorized melanoma samples into three distinct cuproptosis-related subtypes based on the expression profiles of 18 CRGs. Survival analysis revealed significant prognostic differences among these subtypes. Further analysis identified DEGs associated with these subtypes that were involved in cytotoxic production, immune response regulation, and various signaling pathways such as PI3K-Akt, potentially impacting tumor cell metabolism and evasion of immune surveillance. potentially impacting tumor cell metabolism and evasion of immune surveillance. Our research focused on the CRG clusters related DEGs, and through algorithm simulation, we obtained eight significant prognostic signatures and established a prognostic model. Previous studies have established prognostic models for bladder cancer, prostate cancer, hepatocellular carcinoma, and other diseases and shown good predictive ability [34-36]. And we also verified the performance of our prognostic models through survival analysis, ROC curve and independent prognostic analysis, etc. The results indicated that our prognostic model has the ability to group patients according to the risk score and predict the prognosis of patients.

The eight screened-out DEGs related to CRG clusters are CAMK4, TLR8, EIF4E3, CLEC2B, OCA2, SLFN13, SAMD9 and NAIP. Notably, research by Li et al. demonstrated that microRNA-129-5p targeted calmodulin-dependent protein kinase IV (CAMK4) to inhibit the proliferation, migration, and invasion of hepatocytes, suggesting that CAMK4 could mitigate cancer progression by inhibiting the MAPK pathway [37]—a key promoter of tumor growth and angiogenesis. This finding indicated that CAMK4 may be a promising target for melanoma, especially since current treatments like Vemurafenib and Trametinib target the MAPK pathway to control disease progression [10]. Toll-like receptors (TLRs), critical to innate immunity, are garnering attention in immunotherapy. With the development of immunotherapy, the TLRs family has also been paid more and more attention. Motolimod, a TLR8 agonist, has shown potential in preclinical models, underscoring

Figure 6. The validation of the prognostic model. The survival analysis results, risk score distribution, survival status, the expression of genes related to prognosis in the high and low risk groups, and AUC of all samples (**A, D, G, J, M**), training set (**B, E, H, K, N**), and test set (**C, F, I, L, O**).

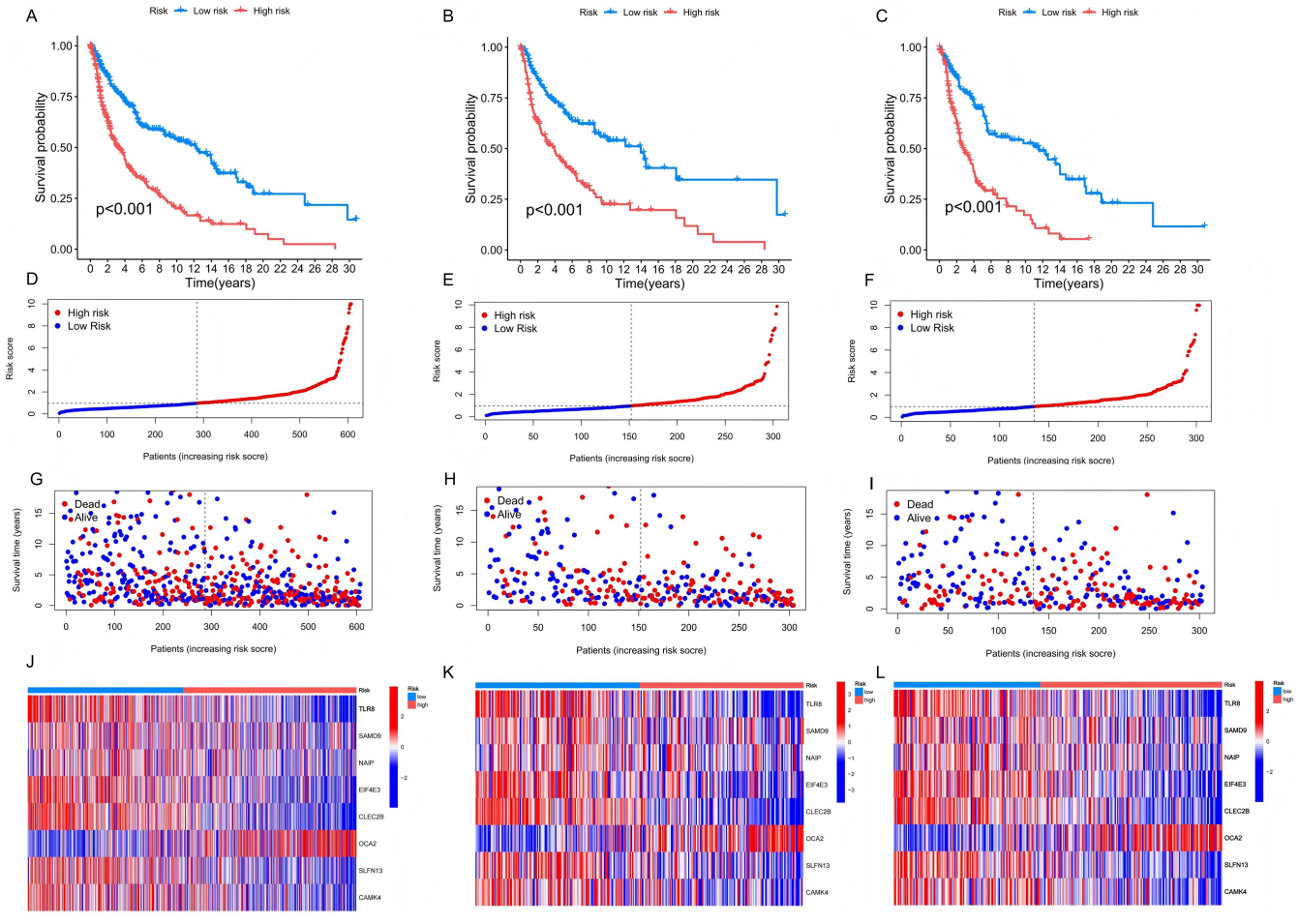

the relevance of the TLRs in cancer treatment, particularly as resistance to existing therapies increases [38]. With the targeting and immune therapy of melanoma, drug resistance is gradually increasing. The development or combination of new drugs may improve the therapeutic effect. Another noteworthy gene, EIF4E3, part of the EIF4E family, acts as a tissue-specific tumor suppressor by binding to the methyl-7-guanosine cap, thus preventing carcinogenic transformation [39]. CLEC2B, a marker identified in various cancers and linked to immune response regulation [40], has been shown to act as a protective factor in melanoma [41]. This suggested its potential utility as a therapeutic target, possibly enhancing immune response against tumor cells. The Schlafen (SLFN) gene family, associated with immune cell differentiation and regulation, showed varied impacts across different cancers. For example, high SLFN13 expression correlated with poor prognosis in gastric cancer [42], yet appeared as a low-risk factor in our melanoma studies, potentially due to epigenetic modifications. This indicated the complex role of SLFN genes in cancer and the need for further investigation. OCA2, associated with pigmentation, has been linked to an increased risk of familial melanoma [43] and cutaneous squamous cell carcinoma [44]. This suggested its role in melanoma progression and potential as a therapeutic target. SAMD9 mutations were implicated in various diseases, including myelodysplastic syndrome (MDS), esophageal cancer, and lung cancer. Research indicated that SAMD9 suppression could slow glioblastoma progression, highlighting its role in cancer development and as a potential therapeutic target [45, 46]. Lastly, the neuronal apoptosis inhibitor protein (NAIP), part of the inhibitor of apoptosis protein (IAP) family, was known to suppress apoptosis. Research by Yang et al. showed that tumor suppressor p53 regulates miR-15a to reduce NAIP expression, thereby enhancing apoptosis in breast cancer cells. This finding aligns with earlier studies suggesting that increasing IAP expression can re-sensitize cancer cells to apoptotic signals, offering new avenues for cancer therapy. This highlighted the potential of targeting IAP pathways, including NAIP, as a strategy for inducing cancer cell apoptosis and improving therapeutic outcomes [47-49]. These findings collectively underscored the potential of these genes as tar-

Figure 7. The clinical applicability of the prognostic model. (**A-B**) The results of univariate and multivariate Cox regression analysis prove that the risk score has independent predictive value. (**C**) The nomogram was used to calculate the survival rates of 1-, 3-, and 5-years for patients with melanoma. (**D**) Calibration curve for nomogram.

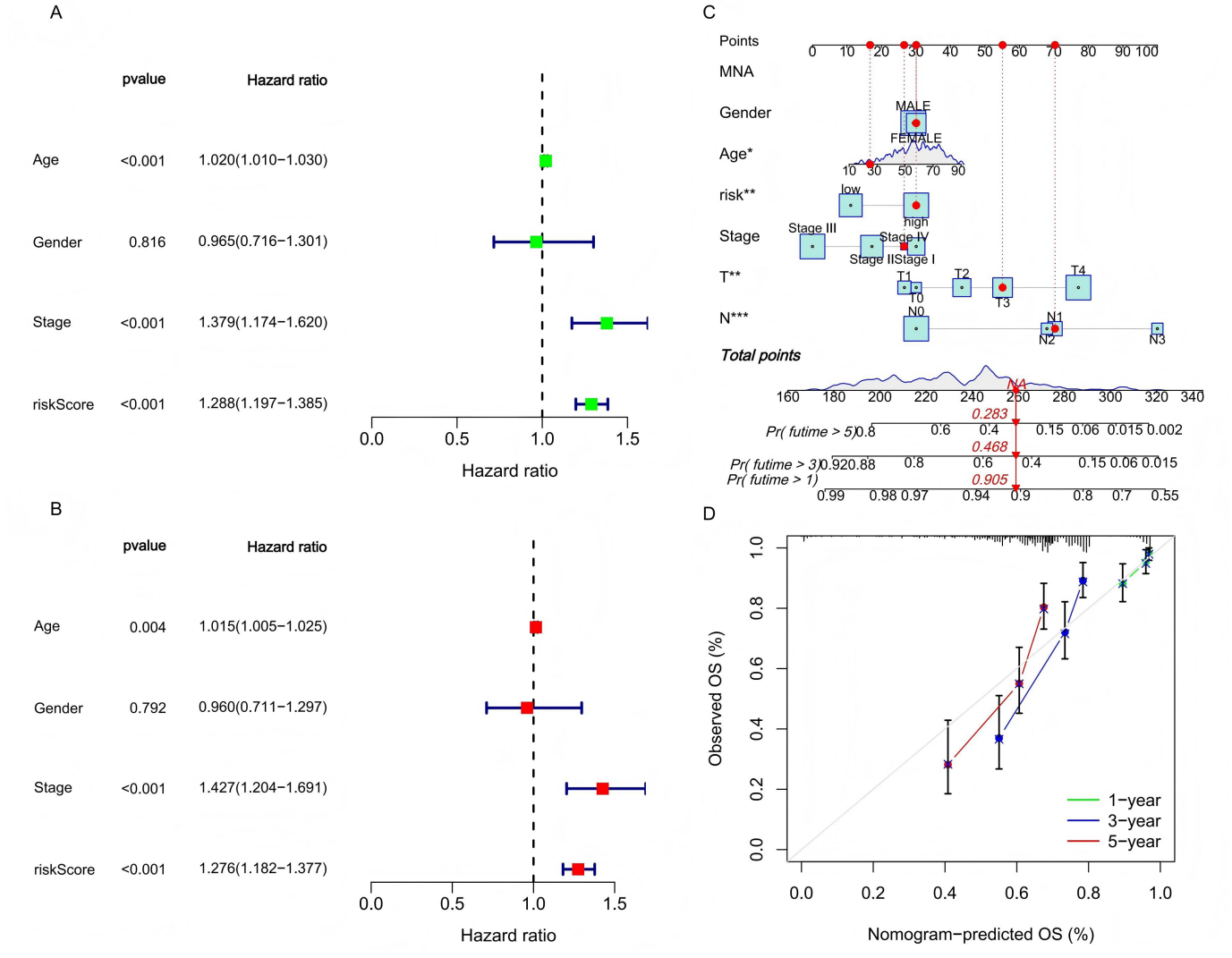

gets for melanoma treatment, necessitating further studies to fully understand their roles and therapeutic potential in the tumor microenvironment and beyond.

TME consists of tumor cells, immune cells, and cytokines, forming an ecosystem that plays a critical role in tumor development, growth, and metastasis [50]. With the advancement of ICB therapies, the study of immune cells, cytokines, and immune mechanisms within the TME has deepened [51]. In our study, we observed a significant negative correlation between risk scores and the infiltration levels of CD8+ T cells, activated memory CD4+ T cells, M1 macrophages, and plasma cells. Macrophages can be polarized into two types based on their phenotype and secreted cytokines: M1 and M2. M1 macrophages secrete tumor-killing agents such as reactive oxygen species, nitric oxide, IFN-γ, and Fas ligand (FasL), and they also recruit other tumor-specific immune cells through chemokine secretion, playing a key role in anti-tumor responses [52]. Similarly, activated memory CD4+ T helper (Th1) cells and CD8+ T cells are crucial for establishing long-term immune memory, which triggers a rapid cytotoxic response upon re-exposure to tumor cells. These immune cells are essential for the long-term remission of melanoma [53, 54]. A disruption in the balance between tumor cells and the host immune response may lead to the progression of melanoma, contributing to the poorer prognosis seen in high-risk groups. These observations are critical for understanding the molecular underpinnings that differentiate prognostic outcomes in melanoma, providing a basis for targeted therapeutic interventions.

In addition, we evaluated the TME of the high-risk and low-risk groups based on the ESTIMATE algorithm. The results showed that the stromal, immune, and ESTIMATE scores were significantly higher in the low-risk group compared to the high-risk group, suggesting that the low-risk group had better immune defense and response capabilities. However, contrary to our expectations, the TIDE score for the low-risk group was higher, indicating a greater likelihood of immune escape in this group. This apparent paradox underscores the complex and dual-nature role of immune responses in melanoma progression. Melanoma is widely recognized for its high immunogenicity, often generating a substantial number of neoantigens through mechanisms such as chromosomal instability, high mutation burden, and structural variants. These tumor-specific antigens can initiate potent innate and adaptive immune reactions, recruiting lymphocytes and other immune mediators into the tumor bed, which is reflected in the high immune scores observed.However, the very intensity of this immune pressure drives the selection of tumor clones capable of exploiting regulatory pathways to evade destruction. Melanoma cells can engage a variety of resistance mechanisms, including the upregulation of immune checkpoint molecules (e.g., PD-L1, CTLA-4), recruitment of immunosuppressive cells (such as Tregs, MDSCs, or M2 macrophages), and secretion of soluble factors that dampen T-cell function. Therefore, an immune-rich microenvironment may not always correlate with productive cytotoxicity; rather, it can represent a battlefield where immune activation and suppression coexist dynamically. The elevated TIDE score in the context of high immune infiltration may thus reflect this dysfunctional state—a TME characterized by abundant but exhausted or inhibited lymphocytes, and active mechanisms of adaptive immune resistance.In summary, the coexistence of high immune scores and high TIDE scores in the low-risk group illuminates the intricate and often contradictory nature of tumor–immune interactions. It suggests that the low-risk group may be dominated by an "immune-inflamed" but poorly effective phenotype, where the immune response is actively suppressed by escape mechanisms. This insight emphasizes the necessity of combining prognostic signatures with functional biomarkers of immune competence to more

Figure 8. Comparison of TME and TMB between high-risk and low-risk groups. (**A**) The correlation between the number of immune cells infiltrated and the eight prognostic signatures and risk score. (**B**) The TME scores of high-risk and low-risk group. (**C-D**) The TMB of high-risk and low-risk group. (**E-F**) K-M survival analysis based on TMB. (**G**) The TIDE scores of two groups.

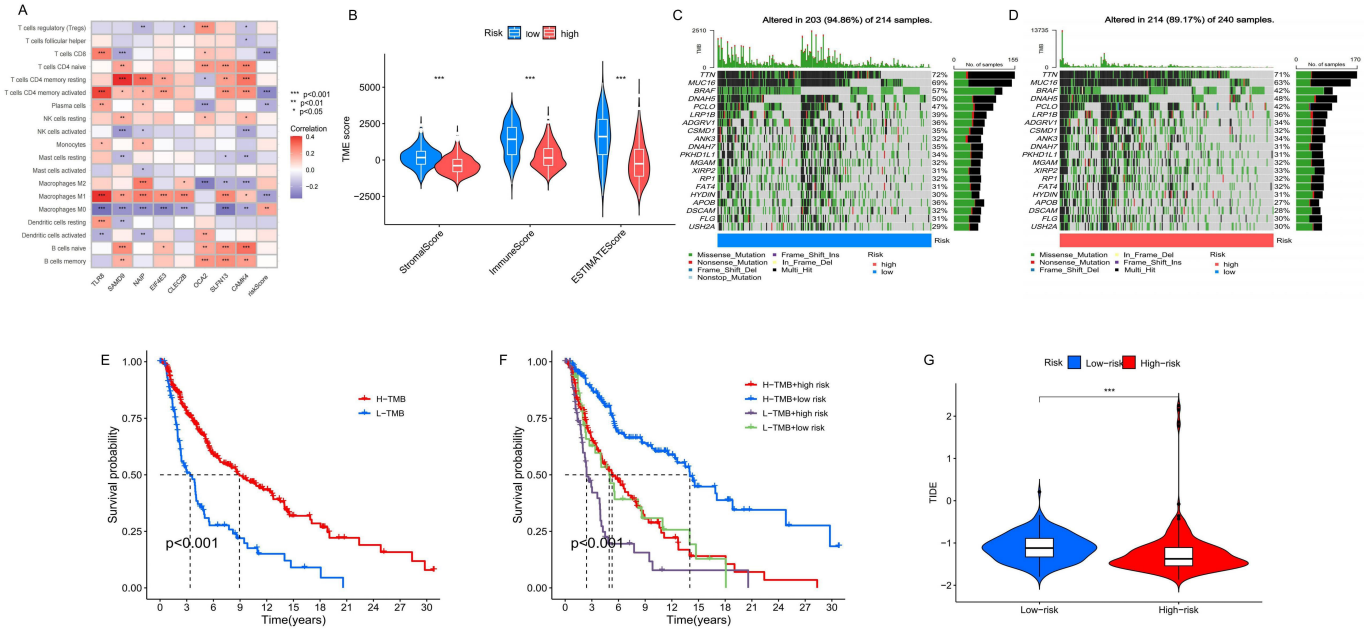

Figure 9. Comparison of sensitivity to chemotherapy or targeted therapy between high-risk and low-risk groups of melanoma patients. (**A**) Axitinib; (**B**) Cisplatin; (**C**) Gemcitabine; (**D**) Methotrexate; (**E**) Nilotinib; (**F**) Rapamycin; (**G**) Sunitinib; (**H**) Temsirolimus; (**I**) Docetaxel; (**J**) Elesclomol; (**K**) Imatinib; (**L**) Thapsigargin.

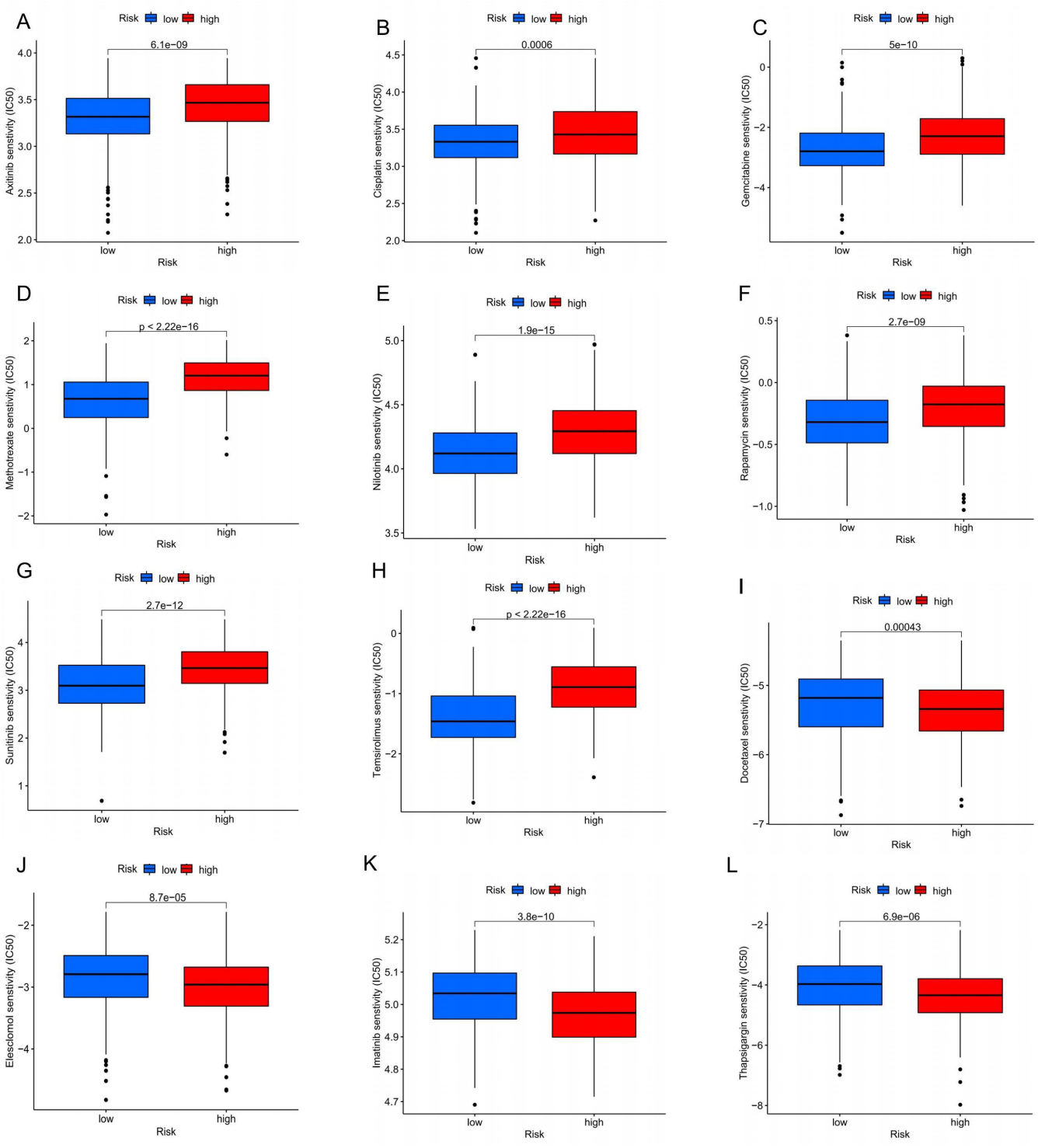

accurately stratify patients and tailor immunotherapeutic strategies [52].

Despite these findings, our study has some limitations. First, the relationship between CRGs and melanoma development remains unclear and warrants further investigation. Additionally, our analysis is based on retrospective clinical samples, and further prospective studies are needed to validate the clinical utility of our prognostic model.

Conclusion

In conclusion, we identified eight prognostic signatures from differentially expressed genes associated with CRG clusters and developed a prognostic model for melanoma patients. This model offers valuable insights into the immune landscape, prognosis, and potential clinical treatment options, serving as a useful reference for guiding personalized melanoma therapies.

Abbreviations

Area under the curve: AUC; Biological Process: BP; Calmodulin-dependent protein kinase IV: CAMK4; Cuproptosis-related genes: CRGs; Cytotoxic T lymphocyte antigen 4: CTLA4; Copy number variation: CNV; Differentially expressed genes: DEGs; Fas ligand: FasL; Gene set variation analysis: GSVA; Gene Expression Omnibus: GEO; Genomics of Drug Sensitivity in Cancer: GDSC; Immune checkpoint blockade: ICB; Inhibitor of apoptosis protein: IAP; Half-maximal inhibitory concentration: IC50; Kaplan-Meier: K-M; Least absolute shrinkage and selection operator: LASSO; Molecular Function: MF; Myelodysplastic syndrome: MDS; Neuronal apoptosis inhibitor protein: NAIP; Principal component analysis: PCA; Regulated cell death: RCD; Receiver operating characteristic: ROC; Single sample gene-set enrichment analysis: ssGSEA; The Cancer Genome Atlas: TCGA; Tricarboxylic acid: TCA; Tumor microenvironment: TME; Tumor mutation burden: TMB; Tumor immune dysfunction and exclusion: TIDE; Toll-like receptors: TLRs; T helper cell 1: Th1

Author Contributions

Zishen Xia, Nan Gao and Jianwen Wang contributed equally to this work as co-first authors, participating in data curation, formal analysis, methodology development, software implementation, visualization, and manuscript writing. Lizhao Yan, Cong Ma, and Kangwei Wang were responsible for reviewing the conceptual design, writing the article, and proofreading. Yuxiong Weng conceived the study, overseeing the study design, writing, data acquisition, analysis, and interpretation. All authors read and approved the final manuscript.

Acknowledgements

Not Applicable.

Funding Information

Not Applicable.

Ethics Approval and Consent to Participate

Not Applicable.

Competing Interests

The authors declare that they have no existing or potential commercial or financial relationships that could create a conflict of interest at the time of conducting this study.

Data Availability

The data that support the findings of this study are available in the following repositories: TCGA [http://cancergenome.nih.gov], GEO: [https://www.ncbi.nlm.nih.gov/geo], TIDE [http://tide.dfci.harvard.edu], GDSC [https://www.cancerrxgene.org]. These data were derived from resources available in the public domain and are freely accessible under their respective usage guidelines.

References

[1] Shain AH, & Bastian BC. (2020). Author Correction: From melanocytes to melanomas. Nature Reviews Cancer, 20(6), 355-355. https://doi.org/10.1038/s41568-020-0269-7

[2] Long GV, Swetter SM, Menzies AM, Gershenwald JE, & Scolyer RA. (2023). Cutaneous melanoma. The Lancet, 402(10400), 485-502. https://doi.org/10.1016/S0140-6736(23)00821-8

[3] Schadendorf D, Fisher DE, Garbe C, Gershenwald JE, Grob J-J, Halpern A, et al. (2015). Melanoma. Nature Reviews Disease Primers, 1(1), 15003. https://doi.org/10.1038/nrdp.2015.3

[4] Corneli P, Zalaudek I, Magaton Rizzi G, & di Meo N. (2018). Improving the early diagnosis of early nodular melanoma: can we do better? Expert Review of Anticancer Therapy, 18(10), 1007-1012. https://doi.org/10.1080/14737140.2018.1507822

[5] Cullen JK, Simmons JL, Parsons PG, & Boyle GM. (2020). Topical treatments for skin cancer. Advanced Drug Delivery Reviews, 153, 54-64. https://doi.org/10.1016/j.addr.2019.11.002

[6] Leonardi, Falzone, Salemi, Zanghì, Spandidos, McCubrey, et al. (2018). Cutaneous melanoma: From pathogenesis to therapy (Review). International Journal of Oncology, 52(4), 1071-1080. https://doi.org/10.3892/ijo.2018.4287

[7] Pavri SN, Clune J, Ariyan S, & Narayan D. (2016). Malignant Melanoma: Beyond the Basics. Plastic and Reconstructive Surgery, 138(2), 330e-340e. https://doi.org/10.1097/prs.0000000000002367

[8] Parra LM, & Webster RM. (2022). The malignant melanoma market. Nat Rev Drug Discov, 21(7), 489-490. https://

doi.org/10.1038/d41573-022-00075-5
[9] Jenkins RW, & Fisher DE. (2021). Treatment of Advanced Melanoma in 2020 and Beyond. Journal of Investigative Dermatology, 141(1), 23-31. https://doi.org/10.1016/j.jid.2020.03.943
[10] Guo W, Wang H, & Li C. (2021). Signal pathways of melanoma and targeted therapy. Signal Transduction and Targeted Therapy, 6(1), 424. https://doi.org/10.1038/s41392-021-00827-6
[11] Winder, M., Virós, A. (2017). Mechanisms of Drug Resistance in Melanoma. In: Mandalà, M., Romano, E. (eds) Mechanisms of Drug Resistance in Cancer Therapy. Handbook of Experimental Pharmacology, vol 249. Springer, Cham. https://doi.org/10.1007/164_2017_17
[12] Witt B, Schaumlöffel D, & Schwerdtle T. (2020). Subcellular Localization of Copper—Cellular Bioimaging with Focus on Neurological Disorders. International Journal of Molecular Sciences, 21(7).
[13] Ge EJ, Bush AI, Casini A, Cobine PA, Cross JR, DeNicola GM, et al. (2022). Connecting copper and cancer: from transition metal signalling to metalloplasia. Nature Reviews Cancer, 22(2), 102-113. https://doi.org/10.1038/s41568-021-00417-2
[14] Wazir SM, & Ghobrial I. (2017). Copper deficiency, a new triad: anemia, leucopenia, and myeloneuropathy. Journal of Community Hospital Internal Medicine Perspectives, 7(4), 265-268. https://doi.org/10.1080/20009666.2017.1351289
[15] Scheiber I, Dringen R, & Mercer JFB. (2013). Copper: Effects of Deficiency and Overload. In A. Sigel, H. Sigel, & R. K. O. Sigel (Eds.), Interrelations between Essential Metal Ions and Human Diseases (10.1007/978-94-007-7500-8_11pp. 359-387). Springer Netherlands. https://doi.org/10.1007/978-94-007-7500-8_11
[16] Aspli KT, Flaten TP, Roos PM, Holmøy T, Skogholt JH, & Aaseth J. (2015). Iron and copper in progressive demyelination – New lessons from Skogholt's disease. Journal of Trace Elements in Medicine and Biology, 31, 183-187. https://doi.org/https://doi.org/10.1016/j.jtemb.2014.12.002
[17] Tsvetkov P, Coy S, Petrova B, Dreishpoon M, Verma A, Abdusamad M, et al. (2022). Copper induces cell death by targeting lipoylated TCA cycle proteins. Science, 375(6586), 1254-1261. https://doi.org/doi:10.1126/science.abf0529
[18] Blockhuys S, Celauro E, Hildesjö C, Feizi A, Stål O, Fierro-González JC, et al. (2016). Defining the human copper proteome and analysis of its expression variation in cancers†. Metallomics, 9(2), 112-123. https://doi.org/10.1039/c6mt00202a
[19] Ackerman CM, Lee S, & Chang CJ. (2017). Analytical Methods for Imaging Metals in Biology: From Transition Metal Metabolism to Transition Metal Signaling. Analytical Chemistry, 89(1), 22-41. https://doi.org/10.1021/acs.analchem.6b04631
[20] Wang Y, Zhang L, & Zhou F. (2022). Cuproptosis: a new form of programmed cell death. Cellular & Molecular Immunology, 19(8), 867-868. https://doi.org/10.1038/s41423-022-00866-1
[21] Kim B-E, Nevitt T, & Thiele DJ. (2008). Mechanisms for copper acquisition, distribution and regulation. Nature Chemical Biology, 4(3), 176-185. https://doi.org/10.1038/nchembio.72
[22] Chan TA, Yarchoan M, Jaffee E, Swanton C, Quezada SA, Stenzinger A, et al. (2019). Development of tumor mutation burden as an immunotherapy biomarker: utility for the oncology clinic. Annals of Oncology, 30(1), 44-56. https://doi.org/10.1093/annonc/mdy495
[23] Zhu Y, Yao S, & Chen L. (2011). Cell Surface Signaling Molecules in the Control of Immune Responses: A Tide Model. Immunity, 34(4), 466-478. https://doi.org/https://doi.org/10.1016/j.immuni.2011.04.008
[24] Auslander N, Zhang G, Lee JS, Frederick DT, Miao B, Moll T, et al. (2018). Robust prediction of response to immune checkpoint blockade therapy in metastatic melanoma. Nature Medicine, 24(10), 1545-1549. https://doi.org/10.1038/s41591-018-0157-9
[25] McGrail DJ, Pilié PG, Rashid NU, Voorwerk L, Slagter M, Kok M, et al. (2021). High tumor mutation burden fails to predict immune checkpoint blockade response across all cancer types. Annals of Oncology, 32(5), 661-672. https://doi.org/10.1016/j.annonc.2021.02.006
[26] Barroso-Sousa R, Jain E, Cohen O, Kim D, Buendia-Buendia J, Winer E, et al. (2020). Prevalence and mutational determinants of high tumor mutation burden in breast cancer. Annals of Oncology, 31(3), 387-394. https://doi.org/10.1016/j.annonc.2019.11.010
[27] Hayward NK, Wilmott JS, Waddell N, Johansson PA, Field MA, Nones K, et al. (2017). Whole-genome landscapes of major melanoma subtypes. Nature, 545(7653), 175-180. https://doi.org/10.1038/nature22071
[28] Nikolaou V, & Stratigos AJ. (2014). Emerging trends in the epidemiology of melanoma. Br J Dermatol, 170(1), 11-19. https://doi.org/10.1111/bjd.12492
[29] Lin WM, & Fisher DE. (2017). Signaling and Immune Regulation in Melanoma Development and Responses to Therapy. Annual Review of Pathology: Mechanisms of Disease, 12(Volume 12, 2017), 75-102. https://doi.org/https://doi.org/10.1146/annurev-pathol-052016-100208
[30] Sun J, Carr MJ, & Khushalani NI. (2020). Principles of Targeted Therapy for Melanoma. Surgical Clinics of North America, 100(1), 175-188. https://doi.org/https://doi.org/10.1016/j.suc.2019.09.013
[31] Renz PF, Ghoshdastider U, Baghai Sain S, Valdivia-Francia F, Khandekar A, Ormiston M, et al. (2024). In vivo single-cell CRISPR uncovers distinct TNF programmes in tumour evolution. Nature, 632(8024), 419-428. https://doi.org/10.1038/s41586-024-07663-y
[32] da Silva DA, De Luca A, Squitti R, Rongioletti M, Rossi L, Machado CML, et al. (2022). Copper in tumors and the use of copper-based compounds in cancer treatment. Journal of Inorganic Biochemistry, 226, 111634. https://doi.org/https://doi.org/10.1016/j.jinorgbio.2021.111634
[33] Tang D, Kang R, Berghe TV, Vandenabeele P, & Kroemer G. (2019). The molecular machinery of regulated cell death. Cell Research, 29(5), 347-364. https://doi.org/10.1038/s41422-019-0164-5
[34] Lin Z, Xu Q, Miao D, & Yu F. (2021). An Inflammatory Response-Related Gene Signature Can Impact the Immune Status and Predict the Prognosis of Hepatocellular Carcinoma [Original Research]. Frontiers in Oncology, Volume 11 - 2021. https://doi.org/10.3389/fonc.2021.644416

[35] Liu H, Gao L, Li J, Zhai T, Xie T, & Xu Y. (2020). Identification and validation of a ferroptosis-related genes based prognostic signature for prostate cancer. bioRxiv.
[36] Sun J, Yue W, You J, Wei X, Huang Y, Ling Z, et al. (2021). Identification of a Novel Ferroptosis-Related Gene Prognostic Signature in Bladder Cancer [Original Research]. Frontiers in Oncology, Volume 11 - 2021. https://doi.org/10.3389/fonc.2021.730716
[37] Li Z, Lu J, Zeng G, Pang J, Zheng X, Feng J, et al. (2019). MiR-129-5p inhibits liver cancer growth by targeting calcium calmodulin-dependent protein kinase IV (CAMK4). Cell Death & Disease, 10(11), 789. https://doi.org/10.1038/s41419-019-1923-4
[38] Frega G, Wu Q, Le Naour J, Vacchelli E, Galluzzi L, Kroemer G, et al. (2020). Trial Watch: experimental TLR7/TLR8 agonists for oncological indications. OncoImmunology, 9(1), 1796002. https://doi.org/10.1080/2162402X.2020.1796002
[39] Osborne MJ, Volpon L, Kornblatt JA, Culjkovic-Kraljacic B, Baguet A, & Borden KLB. (2013). eIF4E3 acts as a tumor suppressor by utilizing an atypical mode of methyl-7-guanosine cap recognition. Proceedings of the National Academy of Sciences, 110(10), 3877-3882. https://doi.org/doi:10.1073/pnas.1216862110
[40] Li X, Tao X, & Ding X. (2022). An integrative analysis to reveal that CLEC2B and ferroptosis may bridge the gap between psoriatic arthritis and cancer development. Scientific Reports, 12.
[41] Gao Y, Li Y, Niu X, Wu Y, Guan X, Hong Y, et al. (2020). Identification and Validation of Prognostically Relevant Gene Signature in Melanoma. BioMed Research International, 2020(1), 5323614. https://doi.org/10.1155/2020/5323614
[42] Chen X, Liang S, Hao J, Wang T, HB, &Liu G, et al. Schlafen family is a prognostic biomarker and corresponds with immune infiltration in gastric cancer. Frontiers in immunology 13, 922138, doi:10.3389/fimmu.2022.922138 (2022).
[43] Hawkes JE, Cassidy PB, Manga P, Boissy RE, Goldgar D, Cannon-Albright L, et al. (2013). Report of a novel OCA2 gene mutation and an investigation of OCA2 variants on melanoma risk in a familial melanoma pedigree. Journal of Dermatological Science, 69(1), 30-37. https://doi.org/10.1016/j.jdermsci.2012.09.016
[44] Chahal HS, Lin Y, Ransohoff KJ, Hinds DA, Wu W, Dai H-J, et al. (2016). Genome-wide association study identifies novel susceptibility loci for cutaneous squamous cell carcinoma. Nature Communications, 7(1), 12048. https://doi.org/10.1038/ncomms12048
[45] Ma W, Jin H, Liu W, Li X, Zhou X, Guo X, et al. (2020). Homeobox B8 Targets Sterile Alpha Motif Domain-Containing Protein 9 and Drives Glioma Progression. Neuroscience Bulletin, 36(4), 359-371. https://doi.org/10.1007/s12264-019-00436-y
[46] Ma W, Zhang K, Bao Z, Jiang T, & Zhang Y. (2021). SAMD9 Is Relating With M2 Macrophage and Remarkable Malignancy Characters in Low-Grade Glioma [Original Research]. Frontiers in Immunology, Volume 12 - 2021. https://doi.org/10.3389/fimmu.2021.659659
[47] Gyrd-Hansen M, & Meier P. (2010). Erratum: IAPs: From caspase inhibitors to modulators of NF-κB, inflammation and cancer (Nature Reviews Cancer (2010) 10 (561-574)). Nature Reviews Cancer, 10(12), 890-890.
[48] Choi J, Hwang YK, Choi YJ, Yoo KE, Kim JH, Nam SJ, et al. (2007). Neuronal apoptosis inhibitory protein is overexpressed in patients with unfavorable prognostic factors in breast cancer. J Korean Med Sci, 22 Suppl(Suppl), S17-23. https://doi.org/10.3346/jkms.2007.22.S.S17
[49] Yang L, Zhao W, Wei P, Zuo W & Zhu S. Tumor suppressor p53 induces miR-15a processing to inhibit neuronal apoptosis inhibitory protein (NAIP) in the apoptotic response DNA damage in breast cancer cell. American journal of translational research 9, 683-691 (2017).
[50] Xiao Y, & Yu D. (2021). Tumor microenvironment as a therapeutic target in cancer. Pharmacology & Therapeutics, 221, 107753. https://doi.org/https://doi.org/10.1016/j.pharmthera.2020.107753
[51] de Visser KE, & Joyce JA. (2023). The evolving tumor microenvironment: From cancer initiation to metastatic outgrowth. Cancer Cell, 41(3), 374-403. https://doi.org/10.1016/j.ccell.2023.02.016
[52] Marzagalli M, Ebelt ND, & Manuel ER. (2019). Unraveling the crosstalk between melanoma and immune cells in the tumor microenvironment. Seminars in Cancer Biology, 59, 236-250. https://doi.org/https://doi.org/10.1016/j.semcancer.2019.08.002
[53] Cui J, Chen Y, Wang HY, & Wang R-F. (2014). Mechanisms and pathways of innate immune activation and regulation in health and cancer. Human Vaccines & Immunotherapeutics, 10(11), 3270-3285. https://doi.org/10.4161/21645515.2014.979640
[54] Woo S-R, Fuertes Mercedes B, Corrales L, Spranger S, Furdyna Michael J, Leung Michael YK, et al. (2015). STING-Dependent Cytosolic DNA Sensing Mediates Innate Immune Recognition of Immunogenic Tumors. Immunity, 42(1), 199. https://doi.org/10.1016/j.immuni.2014.12.015